

Spectrum of the QCD flux tube in 3d SU(2) lattice gauge theory

Bastian B. Brandt

*Institut für Kernphysik, Johannes Gutenberg-Universität Mainz,
Johann Joachim Becher-Weg 45, D-55099 Mainz**

Pushan Majumdar

Dept. of Theoretical Physics, Indian Association for the Cultivation of Science, Jadavpur, Kolkata 700032.[†]

Evidence from the lattice suggests that formation of a flux tube between a $q\bar{q}$ pair in the QCD vacuum leads to quark confinement. For large separations between the quarks, it is conjectured that the flux tube has a behavior similar to an oscillating bosonic string, supported by lattice data for the groundstate $q\bar{q}$ potential. We measure the excited states of the flux tube in 3d SU(2) gauge theory with three different couplings inside the scaling region. We compare our results to predictions of effective string theories.

I. INTRODUCTION

Simulations over the last few years have accumulated strong evidence that gluonic dynamics indeed leads to the formation of a flux tube between test quark and antiquark ($q\bar{q}$) in the vacuum of Yang-Mills theory [1, 2]. This implies a linearly rising potential between quark and antiquark in the QCD vacuum and thus leads to quark confinement. At large $q\bar{q}$ separations, this flux tube is expected to behave like a string. Open bosonic string descriptions of the dynamics of this flux tube have been attempted for a long time [3]. Using the Nambu-Goto (NG) action, first *Alvarez* [4] (in the limit $d \rightarrow \infty$) and later *Arvis* [5] obtained the energy states of the flux tube as

$$E_n(R) = \sigma R \sqrt{1 + \frac{2\pi}{\sigma R^2} \left(n - \frac{1}{24} (d-2) \right)} \quad (1)$$

where σ is the string tension, R the quark-antiquark separation and d the number of space-time dimensions. A closed string description was proposed by Polchinski and Strominger (PS) [6] where they suggested how effective string theory with vanishing conformal anomaly could be formulated in arbitrary dimensions. The spectrum of the string using the PS prescription has been computed in [7, 8, 9]. To order R^{-3} it has been found that the spectrum is universal (depends only on the number of space-time dimensions and the string tension), and to this order it coincides with the NG spectrum. For a calculation of the closed string spectrum on the lattice see [10]. Using symmetry properties of the Polyakov loop correlation function, Lüscher and Weisz (LW) showed that any effective string picture possesses an open-closed duality property [11]. They also showed that demanding this duality constrains the possible string spectra and in particular forbids $1/R^2$ terms in the effective string action.

In the LW formulation too, the spectrum is consistent with the NG spectrum. In 3-dimensions it is exactly the same and in 4-dimensions one undetermined parameter remains which can of course assume the NG value. The NG partition function itself respects open-closed duality. Predictions from these theories can be tested by comparing them to results coming from simulations of pure Yang-Mills theories.

In this Letter we will present a new scheme for measuring observables in simulations of pure Yang-Mills theories. Using this scheme we will accurately measure observables in 3-dimensional SU(2) lattice gauge theory and try to extract the excitation spectrum of the flux tube. For earlier studies of the QCD string spectra using different schemes in both 3- and 4-dimensions for several gauge theories, see [12] and the references therein.

II. PRELIMINARIES

To probe the properties of the flux tube formed between test quark and antiquark, the two observables in pure Yang-Mills theories are the Polyakov loop correlation function and spatio-temporal Wilson loops. While Polyakov loop correlation functions project very strongly onto the ground state, Wilson loops are much more sensitive to the excited states of the flux tube and in addition allows one to couple more strongly to a particular state while suppressing the others, by appropriate choice of the spatial parts of the loop. It is therefore the observable of choice if one wants to study the excitation spectrum of the flux tube.

A. Extraction of the excited states

In 3-dimensions, the states of the oscillating string can be classified by charge-conjugation and parity properties (C, P) [13, 14]. Choosing the spatial parts of the Wilson loops as shown in figure 1, the (C, P) projectors are given

*Electronic address: brandt@kph.uni-mainz.de

[†]Electronic address: tppm@iacs.res.in

by the superpositions

$$\begin{aligned}
\mathbb{S}^{++} &= \mathbb{S}_1 + \mathbb{S}_2 + \mathbb{S}_3 + \mathbb{S}_4 \\
\mathbb{S}^{+-} &= \mathbb{S}_1 + \mathbb{S}_2 - \mathbb{S}_3 - \mathbb{S}_4 \\
\mathbb{S}^{--} &= \mathbb{S}_1 - \mathbb{S}_2 - \mathbb{S}_3 + \mathbb{S}_4 \\
\mathbb{S}^{-+} &= -\mathbb{S}_1 + \mathbb{S}_2 - \mathbb{S}_3 + \mathbb{S}_4
\end{aligned} \tag{2}$$

where $+/-$ stands for even or odd states under C and P . Although in each of the (C, P) channels, there are an infinite number of states, we are going to look only at the ground states and will label these channels as $\{0, 1, 2, 3\}$

respectively. The Wilson loop projecting onto a channel n has the spectral representation

$$W_n(R, T) = \sum_{i=0}^{\infty} \beta_i(R) e^{-E_n^i(R) T}. \tag{3}$$

where E^i are the energies of the states in a given channel. Using Wilson loops with different temporal extents, one obtains the energies and energy differences at leading order as

$$-\frac{1}{T_b - T_a} \ln \left[\frac{W_n(R, T_b)}{W_n(R, T_a)} \right] = E_n(R) + \frac{1}{T_b - T_a} \alpha_n(R) e^{-\delta_n(R) T_a} \left(1 - e^{-\delta_n(R) (T_b - T_a)} \right) \tag{4}$$

$$-\frac{1}{T_b - T_a} \ln \left[\frac{W_n(R, T_b) W_m(R, T_a)}{W_n(R, T_a) W_m(R, T_b)} \right] = \Delta E_{nm}(R) + \frac{1}{T_b - T_a} \alpha_n(R) e^{-\delta_n(R) T_a} \left(1 - e^{-\delta_n(R) (T_b - T_a)} \right) \tag{5}$$

where $T_a < T_b$. In the following, the values obtained from the LHS of eqns.(4) and (5) will be called naïve values and be denoted by $\bar{E}_n(R)$ and $\bar{\Delta E}_{nm}(R)$. The quantities $E_n(R)$ and $\Delta E_{nm}(R)$ will be called corrected values. They, along with α_n and δ_n , are obtained as fit parameters. The fits are done by taking all possible combinations of T_a and T_b and are discussed in more detail in Section D.

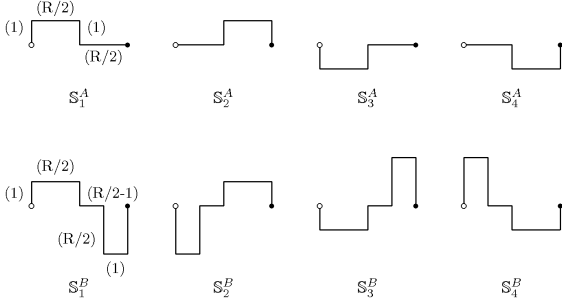


FIG. 1: **Top:** Basic set of operators used to construct (C, P) channels. **Bottom:** Set of operators with stronger coupling to the second excited state.

B. Noise reduction techniques

String like behavior of the flux tube is expected to occur at large $q\bar{q}$ separations. The Wilson loops we measure must therefore extend to large enough R values. Also we see from equations (4) and (5) that to reduce the contaminations due to other states we must either go to large values of T or tune α to small values by appropriate choice of the basis states. The latter method

has been followed in [15] where asymmetric lattices with small temporal extents were used. The former method requires accurate measurements of expectation values of large Wilson loops, made possible recently by the multi-level algorithm, proposed in [16]. This method has been used in [17, 18] to accurately measure the ground state properties of the flux tube. Here we will try to combine both methods by using a slight variant of the multilevel algorithm.

In the multilevel algorithm, intermediate averages are computed for the temporal links by updating certain sub-lattices with the sources on the spatial links of the boundaries of these sub-lattices. The boundaries are held fixed during the sub-lattice updates. We now put the sources on space-like surfaces in the middle of a sub-lattice of thickness $2a$ where a is the lattice spacing. Two temporal links are attached to the two ends of the source which terminates on the space-like surfaces that are fixed during the sub-lattice updates (see fig.2). The advantage is that the sub-lattice updates reduces fluctuations of the sources as well as fluctuations of the temporal links. Moreover, in addition to using multihit on the temporal links, we can now use multihit on the spatial links as well. For further details see [13, 19] and references therein. Adopting the notation in [16], we now define the expectation value of the Wilson loop by

$$\langle W(T) \rangle = \langle \{ \mathbb{L}(0) \}_{\alpha\gamma} \{ \mathbb{T}(a) \cdots \mathbb{T}((T-1)a) \}_{\alpha\beta\gamma\delta} \{ \mathbb{L}(T)^* \}_{\beta\delta} \rangle, \tag{6}$$

where $\mathbb{L}(t)$ is the operator of fig.2 and $\{ \}$ indicates sub-lattice averaged quantities. The only difference from [16] is that now we have $\{ \mathbb{L} \}$ instead of \mathbb{L} . A similar method was used in [20] to measure the static potential and observe string breaking in the adjoint representation.

In most parts of the calculations, the operators $\{ \mathbb{S}_i^A \}$

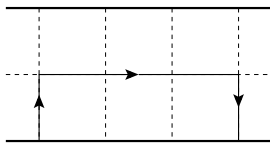


FIG. 2: The source of the Wilson loop in the modified algorithm. The product of the directed lines defines the source. The thick lines are held fixed during sub-lattice updates.

(figure 1 top; see also [14, 19]) are good enough for a reliable signal. However, for the second excited state beyond $\beta = 7.5$ the error reduction was not sufficient and we had to use another set of operators $\{\mathbb{S}_i^B\}$, (figure 1 bottom) with a stronger coupling to that particular excited state. We will henceforth refer to the two sets as set *A* and set *B*, respectively. To check the error reduction with the new set of operators we performed 460 measurements at $\beta = 7.5$ with spatial extents $R = 15 - 20$ using the simulation parameters shown in table I. The resulting relative errors of \bar{E}_2 are also tabulated there. The values for the naïve energies using both sets are plotted in figure 3. For comparison we also plot E_2 , which was calculated from \bar{E}_2^A , in the same region. It is clearly seen that not only do the naïve values of set *B* already coincide with the corrected values of set *A*, they also have much smaller error bars. Set *B* therefore significantly improves the signal for the state \mathbb{S}^{--} .

There are several parameters for the algorithm, that have to be tuned properly in order to achieve the maximal error reduction. For the temporal links we follow the same procedure as outlined in [14]. In addition we now have another parameter which is the number of updates (N_s) for the sub-lattices containing the spatial operators. We found it beneficial for the excited states to have quite a large number of such sub-lattice updates. Since there are only two such sub-lattices for every loop this does not increase the cost of the simulation very much. Table II contains the resulting optimized run parameters and we refer to [13] for details of the optimization.

C. Simulation parameters and lattice scales

Our simulations were done with three different couplings, $\beta = 7.5, 10.0$ and 12.5 (chosen so as to lie in the scaling region) in 3-dimensional $SU(2)$ lattice gauge theory, using usual heatbath sweeps [21], combined with three overrelaxation sweeps. The scale was set by the Sommer parameter r_0 [22], which has been computed for

T	Lat	t_s	N_s	N_t	R	15	16	17	18	19	20
6	36^3	4	18000	1500	A	0.62	0.73	0.85	0.99	1.23	1.60
10	40^3	4	18000	2500	B	0.39	0.45	0.50	0.60	0.77	0.99

TABLE I: **Left:** Parameters of the testruns to compare the operators. **Right:** Relative error of \bar{E}_2 in % for operator sets *A* and *B*.

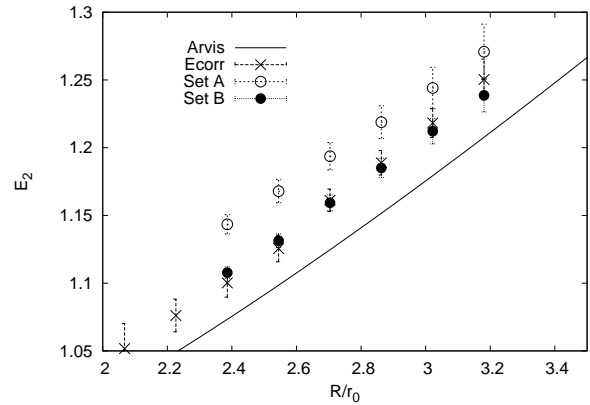


FIG. 3: Comparison of the naïve energy \bar{E}_2 from set *A* and *B*.

these β values with high accuracy in [18]. For each beta value we calculated Wilson loops with four different temporal extents and used cubic lattices.

Our simulation parameters, lattice scales, along with the parameters for the multilevel algorithm are also tabulated in table II.

D. Error analysis and control of the fits

For estimating the error of all the energy values and differences, we used the usual binned jackknife method, with 44, 24, 40 and 40 bins for the lattices L^A , L_A^B , L_B^B and L^C , respectively. We also checked that the errors did not vary by more than a few percent with bin size.

For the energy difference ΔE_{20} at $\beta = 10.0$ and 12.5 we used the results obtained from set *B* for E_2 while the values for E_0 were obtained from set *A*. Since these two values come from independent simulations, we added the individual errors in quadrature to obtain error estimates for ΔE_{20} .

The remaining issue is the control of the fits (4) and (5), and this was done in two ways. For the energies E_n , we expect α to be smaller than the ratio of the degeneracies [27] of the energy states considered and δ should be of the order of the energy gap to the next level in the channel. Similar conclusions hold for the parameters of the energy differences [13, 14] as well. If the resulting fit parameters were far of from these expectations we did not trust the fits. As a second check we plot the expected corrections

$$\Delta = \frac{1}{T_b - T_a} \alpha_n(R) e^{-\delta_n(R) T_a} \left(1 - e^{-\delta_n(R) (T_b - T_a)} \right),$$

obtained with averaged parameters α_n and δ_n against the differences $\bar{\Delta} = E_n - \bar{E}_n$, for all possible combinations of T_a and T_b . We show an example for these fits (ΔE_{10} , $\beta = 7.5$, $R = 11$ and 15) in figure 4. If for some of the values there was a big discrepancy to the expectation $\Delta = \bar{\Delta}$ the fit was also regarded as unreliable (for more details and systematics of the fits see [13] and [14]).

Lat	β	r_0	$a[fm]$	R	$\{S_i\}$	T	$T[fm]$	t_s	size	N_s	N_t	#meas
L^A	7.5	6.2875(10)	0.07952(1)	7 – 20	A	6	0.477	4	38 ³	36000	1500	4400
						10	0.795	4	40 ³		3000	6468
						14	1.113	6	42 ³		9000	11176
						18	1.431	4	54 ³		18000	6512
L_A^B	10.0	8.6602(8)	0.05812(1)	9 – 27	A	8	0.465	6	40 ³	48000	3000	1272, 1272, 1296*
						10	0.581	4	50 ³		3000	2352, 2544, 2568
						14	0.814	6	56 ³		6000	6384, 6216, 6480
						18	1.046	4	54 ³		12000	8664, 8304, 8472
L_B^B	10.0	8.6602(8)	0.05812(1)	9 – 27	B	6	0.349	4	48 ³	48000	1500	2000, 2000**
						8	0.465	6	48 ³		3000	2000, 6000
						10	0.581	4	50 ³		6000	2000, 7960
						14	0.814	6	56 ³		12000	2000, 2000
L^C	12.5	10.916(3)	0.04580(1)	11 – 29	A&B	8	0.366	6	48 ³	36000	2000	1000
						10	0.458	4	50 ³		3000	4000
						14	0.641	6	56 ³		6000	7080
						18	0.824	4	72 ³		12000	2080

TABLE II: Run parameters of the simulations. The number of measurements marked with * corresponds to the R values 9 – 15, 17 – 21, 23 – 27 and the ones marked with ** to 9 – 15, 17 – 27 respectively.

E. Finite volume effects

Finite volume effects are possible due to finite spatio-temporal extents of the lattices. To control the effects due to finite temporal extents, we use four different extents to make sure that any systematic error in our energy values is much lower than our statistical errors.

The dominant corrections due to finite spatial extents are around-the-world glueball exchanges of the form $a(R) \exp(-m_G(L - R))$, where m_G is the glueball mass and L is the spatial extent of the lattice. These are relevant for large values of R . While glueball masses for 3-dimensional SU(2) lattice gauge theory has been studied in [23, 24], the mixing coefficient $a(R)$ is not known. To get an estimate for this coefficient, we did runs at different lattice volumes at $\beta = 5$ (for which m_G has been measured in [24]), varying L by a factor two. Since we did not see any finite size effects in the energies, we concluded, that in the range considered, $a(R)$ is a number of order one.

Using interpolation, we obtain from the data in [24], the glueball masses at $\beta = 7.5$, 10.0 and 12.5 to be 0.856, 0.671 and 0.536 respectively in lattice units. Since our data at large R , with systematic errors under control is only at $\beta = 7.5$, we concentrate on that β value. The only lattice where this correction matters is the $L = 42$ lattice on which we measure Wilson loops with $T = 14$ and R between 7 – 20. On this lattice, the correction ranges between 10^{-9} and 6.7×10^{-9} for R between 18 – 20. The error bars for the wilson loop corresponding to the second excited state are of similar magnitude for $R = 19$ and 20 while for the first excited state, $R = 20$ has a similar error bar. We therefore expect that there can be some correction due to the glueball for these energy values while for all other values, the corrections are well

below our statistical errors.

III. SIMULATION RESULTS

In this section we discuss the results of our simulations, that are tabulated in table III. We compare to the full NG spectrum, eq.(1) and to leading order (LO) and next to leading order (NLO) models which are obtained by truncating the expansion of the square root of (1) in $1/R^2$ at leading order and next to leading order respectively. The LW and PS type string theories give identical results to NLO order. The curves in the plots were drawn using the string tension at $\beta = 12.5$. All the results have been rescaled so that they are visible on a single plot.

A. Energy states

We use the groundstate to determine the string tension and fix an additive constant V_0 , appearing in the potential, by fitting to the form [5]:

$$V(R) = \sigma R \sqrt{1 - \frac{\pi}{12 \sigma R^2}} + V_0 \quad (7)$$

The results of the fits are shown in table IV, where also the values from [18] are shown for comparison. We see that all results agree well within error bars. Also σ and V_0 from both operator sets agree with each other.

In figure 5 the results for the total energies are shown against R/r_0 , together with the predictions of the NG spectrum. The energies are rescaled such that $E_n^{LO} = n$. The results for the groundstate are completely in agreement with the NG predictions. In this case only the curve of the full spectrum is shown since deviations at different orders of the expansion are not visible on this scale.

R	E_0		E_1		E_2	ΔE_{10}		ΔE_{20}
$\beta = 7.5$	$T(18, 14)$	$4T^*$	$T(18, 14)$	$4T^*$	$T(18, 14)^*$	$T(18, 14)$	$4T^*$	$T(18, 14)^*$
7	0.4251(1)	0.42992(8)	0.753(1)	0.773(2)	0.91(7)	0.328(1)	0.302(3)	0.49(7)
8	0.4660(1)	0.47226(9)	0.768(1)	0.784(2)	0.96(6)	0.302(1)	0.284(2)	0.50(6)
9	0.5064(2)	0.5135(1)	0.785(1)	0.797(3)	0.99(5)	0.279(1)	0.267(3)	0.49(5)
10	0.5464(2)	0.5464(2)	0.806(1)	0.804(2)	1.01(4)	0.259(1)	0.257(3)	0.46(4)
11	0.5863(2)	0.5862(3)	0.828(1)	0.826(2)	1.03(3)	0.242(1)	0.240(3)	0.43(7)
12	0.6259(3)	0.6259(3)	0.853(1)	0.850(2)	1.04(2)	0.227(1)	0.224(3)	0.41(2)
13	0.6655(3)	0.6654(4)	0.879(1)	0.876(3)	1.06(2)	0.214(1)	0.211(3)	0.40(2)
14	0.7049(3)	0.7047(5)	0.907(1)	0.904(3)	1.08(2)	0.202(1)	0.199(3)	0.38(2)
15	0.7442(4)	0.7441(5)	0.936(1)	0.933(3)	1.10(2)	0.192(1)	0.189(3)	0.36(2)
16	0.7835(4)	0.7833(6)	0.966(2)	0.963(3)	1.13(1)	0.183(2)	0.180(4)	0.34(1)
17	0.8228(5)	0.8225(7)	0.998(2)	0.995(4)	1.15(1)	0.175(2)	0.172(4)	0.33(1)
18	0.8620(5)	0.8617(7)	1.030(2)	1.027(4)	1.18(1)	0.168(2)	0.165(4)	0.32(1)
19	0.9012(5)	0.9009(8)	1.064(3)	1.061(5)	1.21(1)	0.162(3)	0.160(5)	0.31(1)
20	0.9404(6)	0.9401(8)	1.097(4)	1.095(6)	1.24(2)	0.157(4)	0.155(6)	0.29(2)
$\beta = 10.0$	$T(18, 14)$	$4T^*$	$T(18, 14)$	$3T^*$	$T(10, 8)$	$3T^*$	$T(18, 14)$	
9	0.3160(1)	0.3207(1)	0.571(1)	0.563(4)	0.772(4)	0.770(9)	0.255(1)	Best
11	0.3599(1)	0.3596(5)	0.587(1)	0.567(6)	0.770(3)	0.757(7)	0.227(2)	estimate
13	0.4032(2)	0.4026(8)	0.609(2)	0.588(5)	0.780(3)	0.769(7)	0.206(2)	is
15	0.4460(2)	0.445(1)	0.634(2)	0.613(5)	0.794(4)	0.780(8)	0.188(2)	$E_1 - E_0$
17	0.4884(3)	0.487(1)	0.663(3)		0.809(2)		0.175(3)	$E_2 - E_0$
19	0.5309(3)	0.529(2)	0.694(3)		0.834(3)		0.163(3)	
21	0.5733(4)	0.571(2)	0.726(4)		0.860(3)		0.152(4)	
23	0.6153(5)	0.613(4)	0.757(7)		0.889(4)		0.142(7)	
25	0.6575(8)	0.655(4)	0.79(1)		0.919(6)		0.14(1)	
27	0.699(2)	0.697(4)	0.84(3)		0.954(10)		0.14(3)	
$\beta = 12.5$	$T(18, 14)$	$4T^*$	$T(18, 10)$	$3T^*$	$T(14, 10)$		$T(18, 10)$	
11	0.2540(2)	0.2535(5)	0.472(1)	0.444(9)	0.612(3)		0.218(1)	Best
14	0.2953(3)	0.2945(9)	0.488(2)	0.459(9)	0.613(3)		0.192(2)	estimate
17	0.3359(4)	0.335(1)	0.510(2)	0.481(8)	0.625(3)		0.173(2)	is
20	0.3761(6)	0.374(2)	0.536(3)	0.512(12)	0.644(4)		0.158(3)	$E_1 - E_0$
23	0.4162(9)	0.414(4)	0.566(5)		0.663(5)		0.147(5)	$E_2 - E_0$
26	0.456(1)	0.453(6)	0.593(9)		0.688(7)		0.134(9)	
29	0.496(2)	0.492(10)	0.622(16)		0.707(11)		0.122(16)	

TABLE III: Results of the simulations. The data columns used in the plots have been denoted by a * on their headers. The left column corresponds to the naïve value of loops, obtained from Wilson loops with the temporal extents given in brackets in the header. The right column corresponds to the value from a fit to the form (4),(5), wherever this was possible and the resulting values are expected to have negligible systematic errors. The header $4T$ means, that the values were obtained using fits to all possible combinations of the four different temporal extents, and the header $3T$ means that combinations from the three lowest temporal extents were used. Where these fits did not work and the data may contain significant systematic errors, we have only indicated what our best estimate is. The naïve data serves both for future referencing as well as estimating the corrections due to finite temporal extents. They give useful upper bounds.

For the excited states we were only able to obtain corrected results over a limited range of R , except for E_1 at $\beta = 7.5$ where we have results over the full range.

We see that the corrected values for $\beta = 7.5$ follow the Nambu curves quite well. In the region where we are able to obtain corrected energies for all values of β , we see good agreement between the different β values. At smaller values of R where the difference between the NG, LO and NLO curves are visible, the data seems to favor the NG curve.

B. Energy differences

We now turn to the energy differences which are more sensitive to subleading properties of the flux tube. In addition they have the advantage that the constant V_0 does not contribute. The results for the energy differences ΔE_{10} and ΔE_{20} are shown in figure 6.

We were able to obtain corrected values using eq.(5) only for ΔE_{10} at $\beta = 7.5$. That data set seems to follow the NG curves quite nicely. For ΔE_{20} , our best estimates are the naïve values from eq.(5) with $T_a = 14$ and $T_b = 18$. Nevertheless we expect very little systematic effects

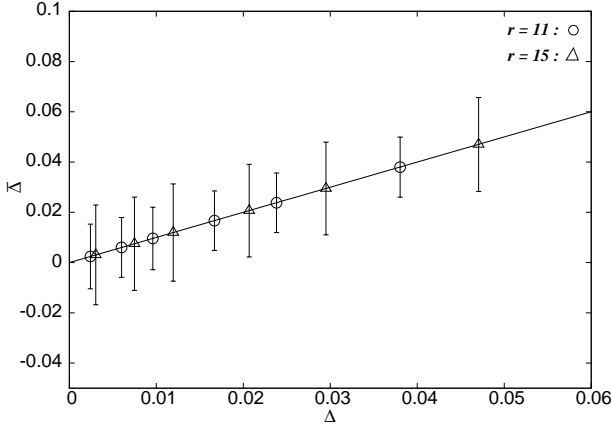


FIG. 4: Cross check of the fits; ΔE_{10} , $\beta = 7.5$.

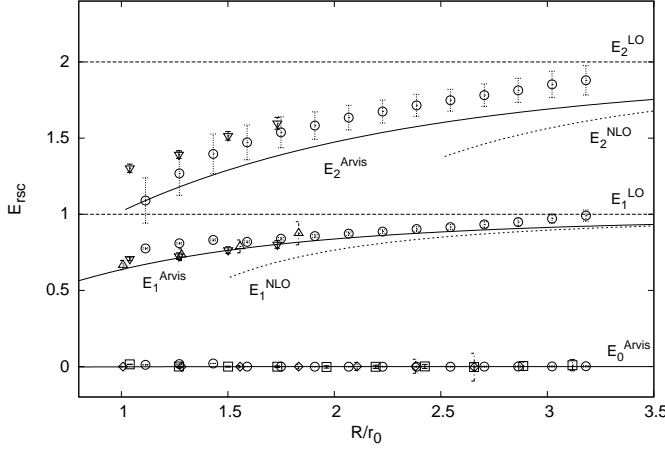


FIG. 5: Results for the total energies E_n . The \circ 's are the values for $\beta = 7.5$, \square 's for $\beta = 10.0$ and \diamond 's for $\beta = 12.5$. ∇ are corrected values for $\beta = 10.0$ and \triangle for $\beta = 12.5$. The results have been rescaled, such that $E_n^{\text{LO}} = n$. The labeling of the lines are as defined in the text.

in these results as the physical temporal extents for these loops are $> 1\text{fm}$. Again we see that the NG curve is favored by the data.

For ΔE_{10} at $\beta = 10.0$ and 12.5 , our best estimates come from the difference $E_1 - E_0$ with the errors being calculated in quadrature. Even though this gives larger error bars, especially at $\beta = 12.5$, we see that both data sets are consistent with $\beta = 7.5$ values.

For ΔE_{20} at $\beta = 10.0$ and 12.5 , the physical temporal extents of the loops are not large enough that the higher order corrections, unaccounted for in equations (4) and (5), are negligible. Nevertheless, at $\beta = 10.0$, where it was possible at least partly to take into account the corrections, we see the trend of the data is to follow the NG curve. For $\beta = 12.5$, where even that was not possible, the data contains systematic errors and we have not plotted it.

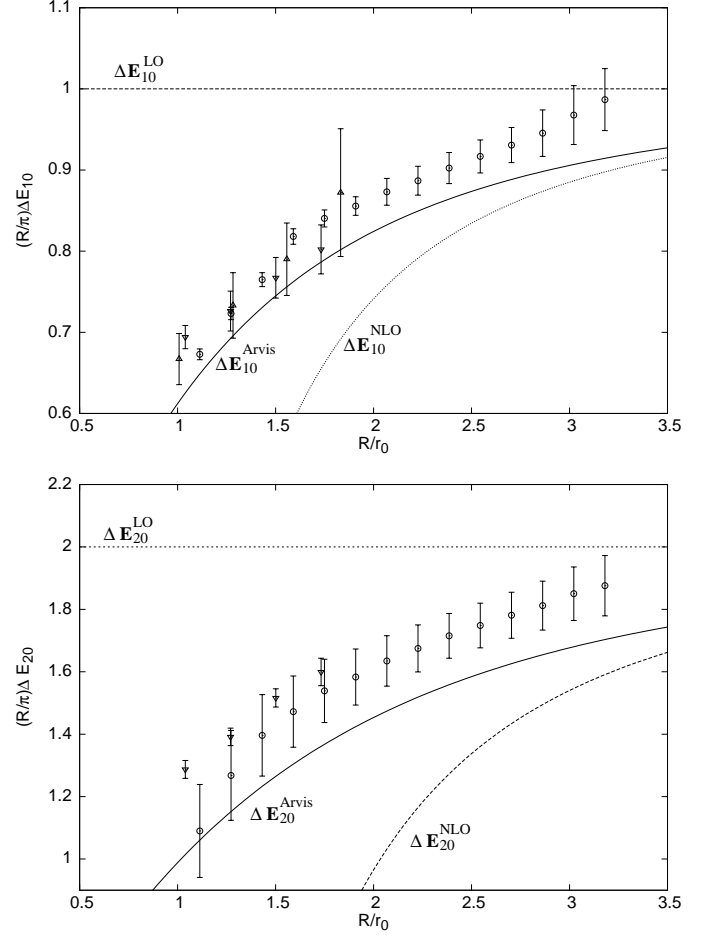


FIG. 6: **Top:** Results for the energy difference ΔE_{10} . **Bottom:** Results for the difference ΔE_{20} . The mapping of the curves and the points is the same as in the plot for the total energies.

IV. CONCLUSIONS

In this Letter we have looked at a variant of the multi-level error reduction scheme suitable for studying the excited states of the QCD flux tube. Using this scheme we have looked at the excited states of the flux tube at three different couplings for $q\bar{q}$ separations between 0.5 and 1.7 fm .

Compared to measurements with the older method [14], we have seen very significant improvements due to the new measurement process. It has been possible to increase the range of R by more than 50% . Since the error in ΔE grows roughly proportional to R^2 , this would be very hard to achieve by increasing computing power alone. Compared to [14], the errors on E_1 and ΔE_{10} have been reduced by a factor between 2 and 3 in the overlapping range of R . This would also be very hard to achieve by increasing statistics alone. Both of these observations clearly demonstrate the superiority of the new measurement process over the older one. Moreover

using the older method we did not have a signal for the second excited state whereas we do have a reasonable measurement now at least for one β value.

Our results seem to indicate that in this scheme, with our basis, upto the values of R we have considered, one needs temporal extents of about 1 fm to make sure that the corrections due to the higher states are well under control. Wherever this criterion has been met, we have seen that the data follows the NG curve.

The corrected data sets for different β values seem to fall on top of each other indicating that there is very little effect due to finite lattice spacing. As such it seems to be much more important to go to larger temporal extents than finer lattices.

Unfortunately our data is still not good enough to distinguish between NG, LW and PS type string theories as that would require a sensitivity at the level of R^{-5} . Deviations from the NG predictions at higher orders have recently been reported in [25] for gauge duals of random percolation problems.

This was our first attempt to show how to combine the two powerful techniques of multi-level error reduction

and sophisticated sources for Wilson loops. Using this we have been able to go to much larger values of R and T than was possible before. For ruling out different string models, the error bars will have to be reduced by at least an order of magnitude. That at the moment looks like a project for the future.

V. ACKNOWLEDGMENTS

The simulations were distributed over three different computational facilities, namely the computing resources of the Westfälische Wilhelms-Universität Münster (organized with the condor system [26]), where this study was started, the teraflop Linux cluster KABRU at IMSc, Chennai and the Linux cluster LC2 at the ZDV of the Johannes Gutenberg-Universität Mainz. We are indebted to the institutes for these facilities. We would also like to thank P. Weisz and H. Wittig for useful discussions on finite size effects for Wilson loops. B.B. is funded by the DFG via the SFB 443.

-
- [1] G. S. Bali, Phys. Rep. **343**, 1 (2001).
 - [2] M. Caselle, M. Pepe, A. Rago, JHEP **0410**, 005 (2004); B. Bringoltz and M. Teper Phys. Lett. **B645**, 383 (2007).
 - [3] P. Goddard *et. al.*, Nucl. Phys. **B 56**, 109 (1973).
 - [4] O. Alvarez, Phys. Rev. **D24**, 440 (1981).
 - [5] J.F. Arvis, Phys. Lett. **127B**, 106 (1983).
 - [6] J. Polchinski and A. Strominger, Phys. Rev. Lett. **67**, 1681 (1991).
 - [7] J.M. Drummond, hep-th/0411017; hep-th/0608109.
 - [8] N.D. Hari Dass and P. Matlock, hep-th/0606265; hep-th/0611215; hep-th/0612291.
 - [9] F. Maresca, Ph.D Thesis, Trinity College, Dublin, 2004; J. Kuti, (unpublished).
 - [10] A. Athenodorou, B. Bringoltz and M. Teper, Phys. Lett. **B656**, 132 (2007) arXiv:0709.0693.
 - [11] M. Lüscher, P. Weisz, JHEP **0407**, 049 (2004).
 - [12] J. Kuti, in *Proceedings of the XXIIIrd International Symposium on Lattice field theory*, PoS(Lattice2005), 001 (2005).
 - [13] B.B. Brandt, Diploma thesis, Westfälische Wilhelms-Universität Münster, 2008.
 - [14] P. Majumdar, Nucl. Phys. **B664**, 213 (2003) hep-lat/0211038; hep-lat/0406037 (2004)
 - [15] J. Juge, J. Kuti and C. Morningstar, Phys. Rev. Lett. **90**, 161601 (2003); in *Proceedings of Wako 2003*, Color confinement and hadrons in quantum chromodynamics, 221, hep-lat/0312019; in *Proceedings of Wako 2003*, Color confinement and hadrons in quantum chromodynamics, 233, hep-lat/0401032.
 - [16] M. Lüscher and P. Weisz, JHEP **0109**, 010 (2001).
 - [17] M. Lüscher and P. Weisz, JHEP **0407**, 014 (2004).
 - [18] N. D. Hari Dass and P. Majumdar, Phys. Lett. **B658**, 273 (2007) hep-lat/0702019; JHEP **0610**, 020 (2006) hep-lat/0608024
 - [19] B.B. Brandt and P. Majumdar, in *Proceedings of the XXVth International Symposium on Lattice field theory*, PoS(Lattice2007), 027 (2007) arXiv:0709.3379.
 - [20] S. Kratochvila, Ph. de Forcrand, Nucl. Phys. **B671**, 103 (2003) hep-lat/0306011.
 - [21] A. Kennedy and B. Pendleton, Phys. Lett. **156B**, 393 (1985)
 - [22] R. Sommer, Nucl. Phys. **B411**, 839 (1994) hep-lat/9310022.
 - [23] C. Michael, J. Phys. G : Nucl. Phys. **13**, 1001 (1987).
 - [24] M. J. Teper, Phys. Rev. **D59**, 014512 (1999) hep-lat/9804008.
 - [25] P. Giudice, F. Gliozzi and S. Lottini, JHEP **0903**, 104 (2009) arXiv:0901.0748.
 - [26] <http://www.condorproject.org/>, ©1990-2009 Condor team, CSD university of Wisconsin, Madison, WI.
 - [27] At the order where we are comparing the data with the theory, the degeneracies are the same as in the free theory [17]

β	7.5 set A	[18]	10.0 set A	10.0 set B	[18]	12.5 set A	12.5 set B	[18]
σ	0.03867(7)	0.038566(6)	0.0206(2)	0.0210(4)	0.020606(4)	0.0128(4)	0.0129(4)	0.012742(17)
V_0	0.1730(5)		0.145(3)	0.139(6)		0.124(4)	0.124(4)	

TABLE IV: Results for the string tension σ and the regularization constant V_0 . The values [18] are the reference results for the string tension.